

Natural convection in a parallel-plate vertical channel with discrete heating by two flush-mounted heaters: effect of the clearance between the heaters

Bugra Sarper¹ · Mehmet Saglam² · Orhan Aydin² · Mete Avci²

Received: 14 March 2017 / Accepted: 16 October 2017 / Published online: 31 October 2017
© Springer-Verlag GmbH Germany 2017

Abstract In this study, natural convection in a vertical channel is studied experimentally and numerically. One of the channel walls is heated discretely by two flush-mounted heaters while the other is insulated. The effects of the clearance between the heaters on heat transfer and hot spot temperature while total length of the heaters keeps constant are investigated. Four different settlements of two discrete heaters are comparatively examined. Air is used as the working fluid. The range of the modified Grashof number covers the values between 9.6×10^5 and 1.53×10^7 . Surface to surface radiation is taken into account. Flow visualizations and temperature measurements are performed in the experimental study. Numerical computations are performed using the commercial CFD code ANSYS FLUENT. The results are represented as the variations of surface temperature, hot spot temperature and Nusselt number with the modified Grashof number and the clearance between the heaters as well as velocity and temperature variations of the fluid.

Nomenclatures

D	Channel depth [m]
D_h	Hydraulic diameter [m]
g	Gravitational acceleration [m/s^2]
Gr_{Dh}^*	Modified Grashof number
h	Convective heat transfer coefficient [$\text{W/m}^2\text{K}$]
k	Thermal conductivity [W/mK]

L	Channel length [m]
Nu	Nusselt number
q	Heat flux [W/m^2]
s	Clearance between the heaters [m]
t	Thickness [m]
T	Temperature [$^{\circ}\text{C}$]

Greek letters

α	Thermal diffusivity [m^2/s]
β	Thermal expansion coefficient of the fluid [$1/\text{K}$]
ε	Surface emissivity
ν	Kinematic viscosity of the fluid [m^2/s]
ρ	Density [kg/m^3]

Subscripts

<i>cond</i>	Conductive
<i>conv</i>	Convective
<i>cu</i>	Copper
<i>f</i>	Fluid
<i>in</i>	Inlet
<i>ins</i>	Insulator
<i>out</i>	outlet
<i>tot</i>	Total
<i>0</i>	Reference
<i>p</i>	Polycarbonate
<i>rad</i>	Radiative
<i>s</i>	Solid

✉ Orhan Aydin
oaydin@ktu.edu.tr

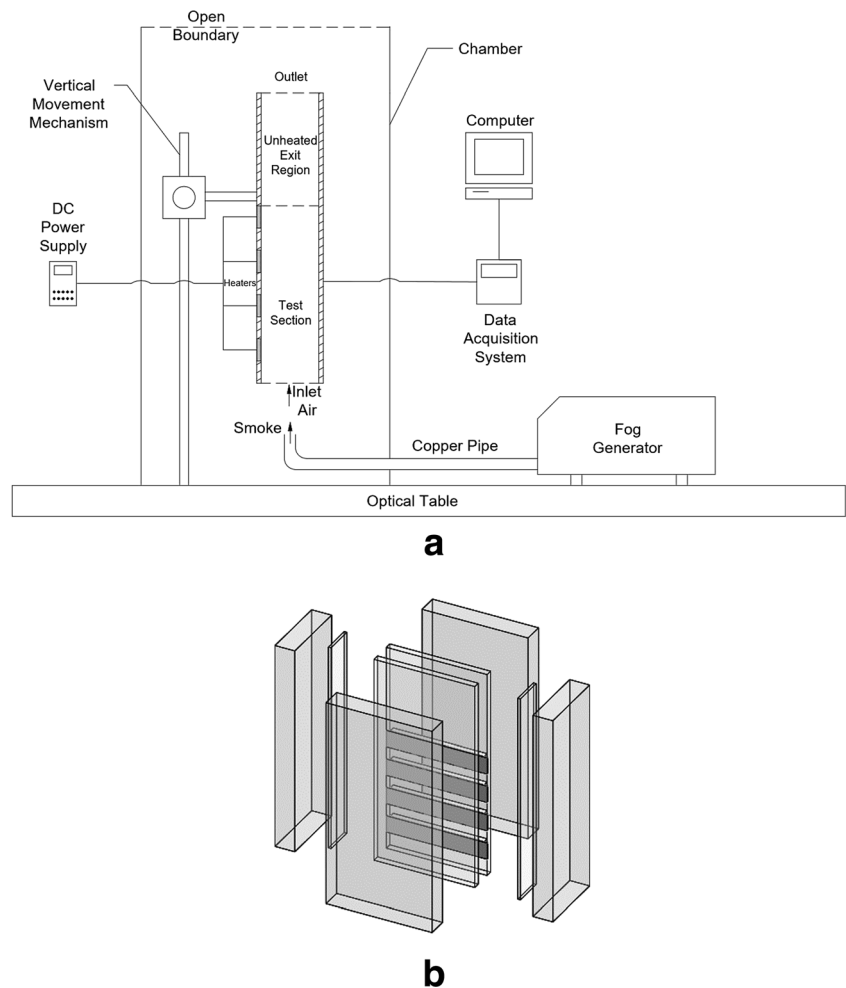
¹ Department of Mechanical Engineering, Gumushane University, 29100 Gumushane, Turkey

² Department of Mechanical Engineering, Karadeniz Technical University, 61080 Trabzon, Turkey

1 Introduction

In recent years, design of electronic devices with higher performance and lower dimensions has become essential. With the development of technology and increase in performance, heat generation by a circuit component also increases, which causes an excessive temperature rise. In order to provide safe

Fig. 1 Schematic of experimental set-up (a), test section (b)



and continuous operation of the system, temperatures of the circuit components need to be kept as low as possible, which should not be exceed the certain limits.

Since natural convection air cooling is a common choice for electronics cooling due to its reliability and easy application, it has received a great deal of research interest. Natural convection in parallel-plate channels is one of the most studied geometries in the existing literature. However, many of those studies assumed differential heating from the sides, i.e. different but uniform temperatures or heat fluxes from the sides. Comparatively, studies on other non-uniform heating from the surface like discrete heating are scarce.

Natural convection in a parallel plate channel with discrete heating was examined in Refs. [1–13]. Conjugate mixed convection with radiation from a vertical plate and in a vertical channel with a discrete heat source were studied numerically by Rao et al. [14–16]. Natural convection in an inclined discretely heated parallel plate channel was studied experimentally for different inclination angles, wall distances, Rayleigh numbers and heater combinations by Manca et al. [17]. The effects of material parameter, Reynolds number, modified Richardson number and channel aspect ratio on turbulent

conjugate mixed convection in a vertical channel with discrete heaters on each wall was analyzed by Mathews and Balaji [18]. Natural and mixed convection in a stack of parallel boards were investigated by Desrayaud [19], and Rao and Narasimham [20]. They focused on the similar geometries with different convection regimes. Conjugate mixed convection from a vertical wall with multiple discrete heat sources was studied numerically by Sawant and Rao [21]. Mixed convection in an inclined channel with discrete heat sources was investigated in Refs. [22, 23]. Laminar aiding and opposing mixed convection in a vertical channel with discrete heat sources was studied numerically by Laouche et al. [24].

Moreover, studies considering wall conduction and surface radiation effects are very scarce, either. Premachandran and Balaji [25] studied the effects of material and surface

Table 1 Thermal conductivities and surface emissivities of the materials

Material	k (W/mK)	ϵ
Copper	387.6	0.05
Polycarbonate	0.217	0.9
XPS Foamboard	0.035	–

properties of channel walls and heaters, modified Grashof and Reynolds numbers on conjugate mixed convection with radiation from a vertical channel with discrete-protruding heaters installed on one of its surfaces. They pointed out that, for an accurate prediction of heat transfer and temperature distribution, radiation heat transfer should not be ignored. Kumar and Rao [26] numerically studied conjugate mixed convection with radiation from a vertical plate with non-identical discrete heat sources. Three discrete heaters were installed on the plate, and the effects of different operating conditions on heater and wall temperatures were investigated. Gavara [27] investigated natural convection in a vertical channel with discrete heaters on opposite conductive walls. Londhe and Rao [28] carried out a numerical study on mixed convection-radiation heat transfer in a vertical channel with three discrete heaters on one of its vertical surface. Recently, the authors of the present study [29] conducted an experimental and numerical study examining the effects of surface radiation on buoyancy induced flow and heat transfer in a discretely heated vertical channel. It was disclosed that radiation heat transfer changed the flow field and affected convective heat transfer positively since it aided buoyancy forces.

There are also optimization studies on enhancement of convection heat transfer from discrete heat sources in different geometries in the literature. Chen et al. [30] performed an experimental study to determine the clearance between heated obstacles on cooling of electronic components. Five equally heated obstacles on the bottom of the channel were installed and five different clearances were analyzed for various values of the Reynolds number. They obtained that heat transfer improved when the distance between heated obstacles was high. Da Silva et al. [31] determined the optimal distribution of discrete heat sources on a vertical wall and on a horizontal plate in natural convection case using the constructal theory. Da Silva et al. [32] optimized the clearances between discrete heat sources in vertical channel via the constructal theory.

Natural convection in channels with discrete heaters at one vertical surface is encountered in many different applications. Electronics cooling is one of them. The discrete heaters resemble the chips on the printed circuit board. The discrete heaters in electronic packages can operate at different times or in different switch time periods. Accordingly, the positions of the heat sources and the clearance between them may vary. Placement of heat sources is very critical for an effective

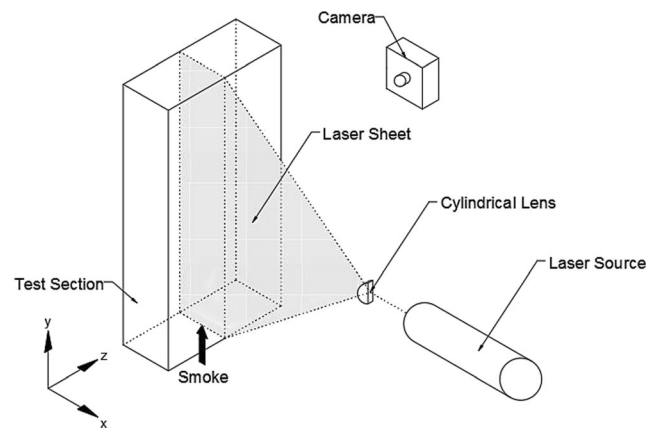


Fig. 2 Flow visualization unit

cooling. For this purpose, four discrete heaters are placed on one of the sidewalls of the channel representing an electronic package and only two of which are thermally active while other two of them are thermally inactive. Four different operating conditions are considered and the clearance between the heaters vary while total heat source length is constant. Therefore, the rationale of the study stands on determining the effect of the clearance between the flush mounted heat sources on thermal performance to reduce the hot spot temperature and to enhance convective heat transfer. It is aimed at experimentally and numerically investigating the buoyancy-induced flow and heat transfer in a vertical channel with two flush-mounted discrete heaters placed on its one wall, including the wall conduction and surface radiation effects.

2 Experimental apparatus and procedure

The schematic of the experimental set-up and the test section are shown in Fig. 1. The experimental set-up consist of a data acquisition system, a computer, a DC power supply, a diode laser, a fog generator, a camera, an optical table, an uninterruptible power supply and the test section. The test cell is placed on an optical table to minimize the vibration effects and oriented by a digital protractor. Experiments are performed in a vertical channel with four identical flush-mounted discrete heaters on its one wall. During the experiments, because of the interest of the present study, only two of the four heaters are powered (“on” position) while the other

Table 2 Grid independence study

Cell number	1,265,616 Cells (20×300×30)	Relative error (%)	1,736,856 Cells (40×300×30)	Relative error (%)	2,235,024 Cells (60×300×30)	Relative error (%)	2,706,264 Cells (80×300×30)
$Nu_{ave,1}$	16.426	4.671	15.693	0.757	15.575	0.238	15.538
$Nu_{ave,2}$	13.201	4.306	12.656	0.676	12.571	0.215	12.544
V_{max}	0.27956	0.014	0.27952	0.007	0.27954	0.01	0.27957

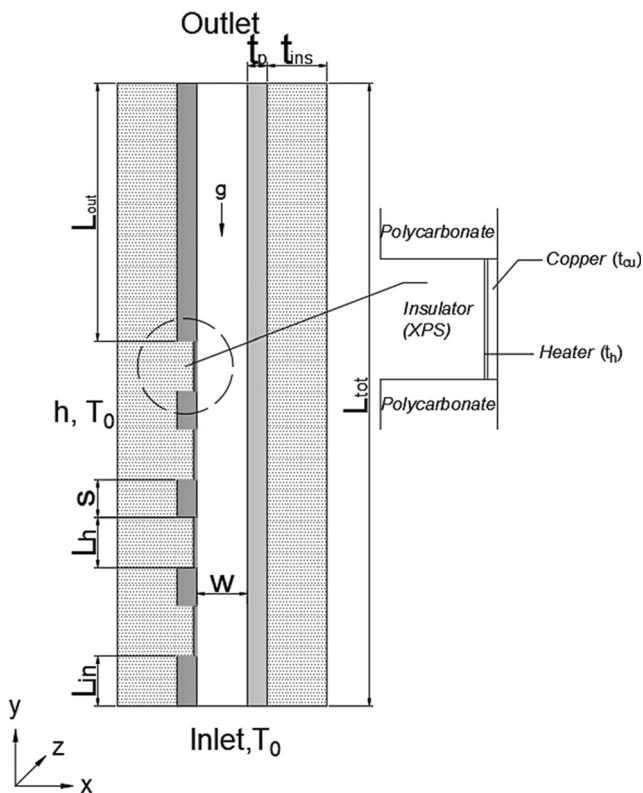


Fig. 3 Schematic of the problem

two are non-powered (“off” position). The remaining surfaces are unheated and thermally insulated. Channel walls are made of 10 mm thick (t_p) polycarbonate plate. Heater surfaces are made of copper with 1.5 mm thickness (t_{cu}), 25.4 mm length

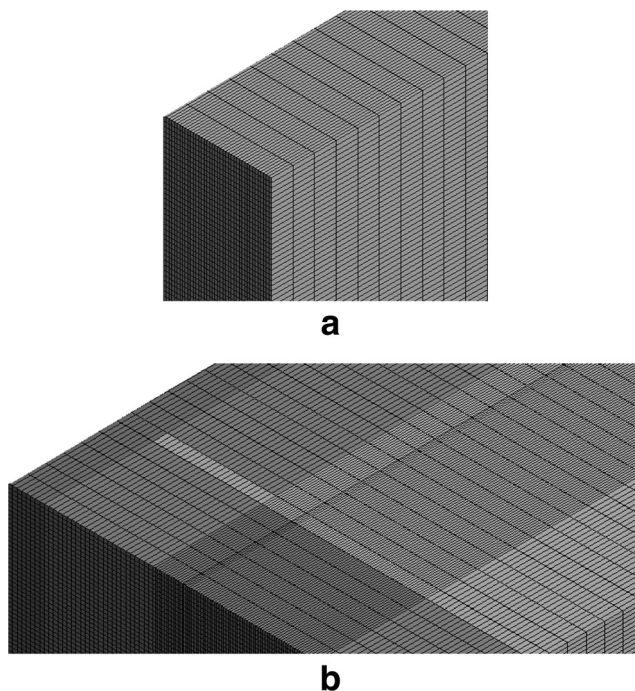


Fig. 4 Grid structure: (a) Fluid domain, (b) fluid domain and all solid bodies

(L_h) and 152.4 mm depth (D). The copper surfaces are heated by polyimide insulated flexible heaters with thickness (t_h) of 0.35 mm. Thermal insulation is ensured with XPS foamboard having a thickness of 30 mm and insulation material is mounted on the back of the flexible heaters and the polycarbonate plates. The total length of the channel (L_{tot}) is 314.33 mm. There is an unheated inlet and outlet section with the dimensions 25.4 mm and 130.18 mm, respectively. The width of the channel (W) is 25.4 mm, and the depth of the channel is equal to the depth of copper plates (D) with the dimension of 152.4 mm. With given dimensions, the hydraulic diameter of the channel (D_h) is 43.54 mm. The copper surfaces are polished, and polycarbonate surfaces are treated as black. Air is used as the working fluid, which enters the channel from the bottom. Thermal conductivities of the materials was measured with Fox 314 thermal conductivity measurement equipment according to ASTM C518 and ISO 8301. Surface emissivities of the polycarbonate plate and polished copper plates can be found in Ref. [33]. Thermal conductivities and surface emissivity values of the materials are given in Table 1.

Three T type thermocouples with a diameter of 0.4 mm are placed 1 mm under each of the copper plates. Eighteen thermocouples are used along the centerline of the polycarbonate plates and two thermocouples are used at the inlet-outlet sections of the channel. Also, 12 thermocouples are located at the back of heaters and insulation material. The input electric power to the flexible heaters is supplied and controlled by a DC modular power system (Agilent 66000A with 66102A power modules). Experiments are performed in an air-conditioned room and the test cell is placed in a chamber in order to minimize environmental impacts. Before starting each experiment, temperature and relative humidity were kept at 24°C and 50% by an air-conditioner. For each measurement, the flow is considered to have reached to the steady state condition when temperature measurements do not change with time anymore Table 2.

Smoke visualization technique is applied to display the flow field. Safex F2010 fog generator, a 50 mW diode laser and a camera are used to visualize the flow domain. After temperatures reach steady state, flow visualization process is started. The smoke is passed through a long copper pipe before being injected to the test section to reduce its temperature. Temperature of the smoke is measured with a thermocouple at the outlet of the copper pipe and it is observed that smoke enters into the test section at a temperature close to the ambient. The sketch of the flow visualization unit is represented in Fig. 2.

The uncertainty analysis is performed by following the methodology described by Holman [34]. Uncertainties of voltage, current and temperature are obtained from the manufacturers’ instruction manuals. Uncertainties of the voltage, current and temperature are 0.008 V, 0.003A and 1°C. In

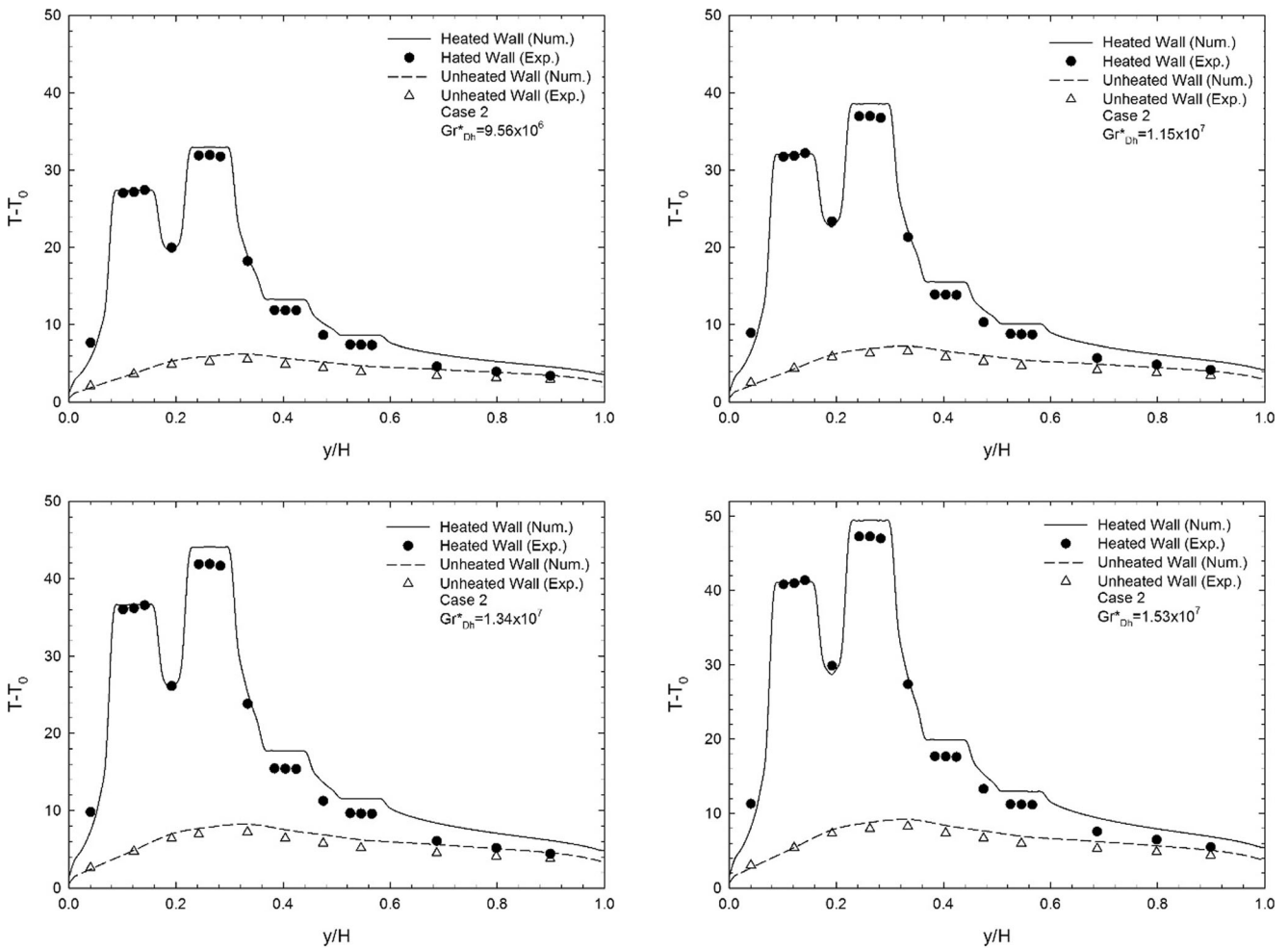


Fig. 5 Comparison of the numerical and experimental results for Case 2

addition, the error caused by the device (Agilent 34972A) for temperature measurements is given as 1.1°C. The maximum uncertainty of the applied power is obtained as 0.575% while the total uncertainty of the temperature measurements is 1.4%.

3 Numerical study

In the numerical part of the study, ANSYS Fluent software is used to solve the governing equations. Flow is assumed to be three dimensional, incompressible, steady and laminar. Constant fluid properties are assumed except for the density change. Density change with temperature that induces buoyancy forces is modelled by adopting Boussinesq approximation. Radiative heat transfer between surfaces and conductive heat transfer inside the solid walls are taken into account. The continuity, momentum, energy and radiation equations are solved via ANSYS Fluent software with the above assumptions. The governing equations can be found in Ref. [33, 35, 36]. The schematic of the problem is shown in Fig. 3.

The modified Grashof number is defined as a function of the volumetric heat generation inside the heaters.

$$Gr_{Dh}^* = \frac{g\beta q' D_h^4 t_h}{k\nu^2} \tag{1}$$

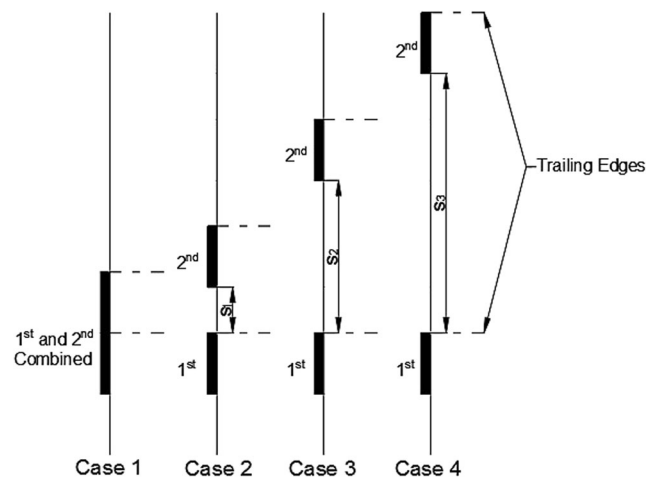


Fig. 6 Sketch of the cases tested

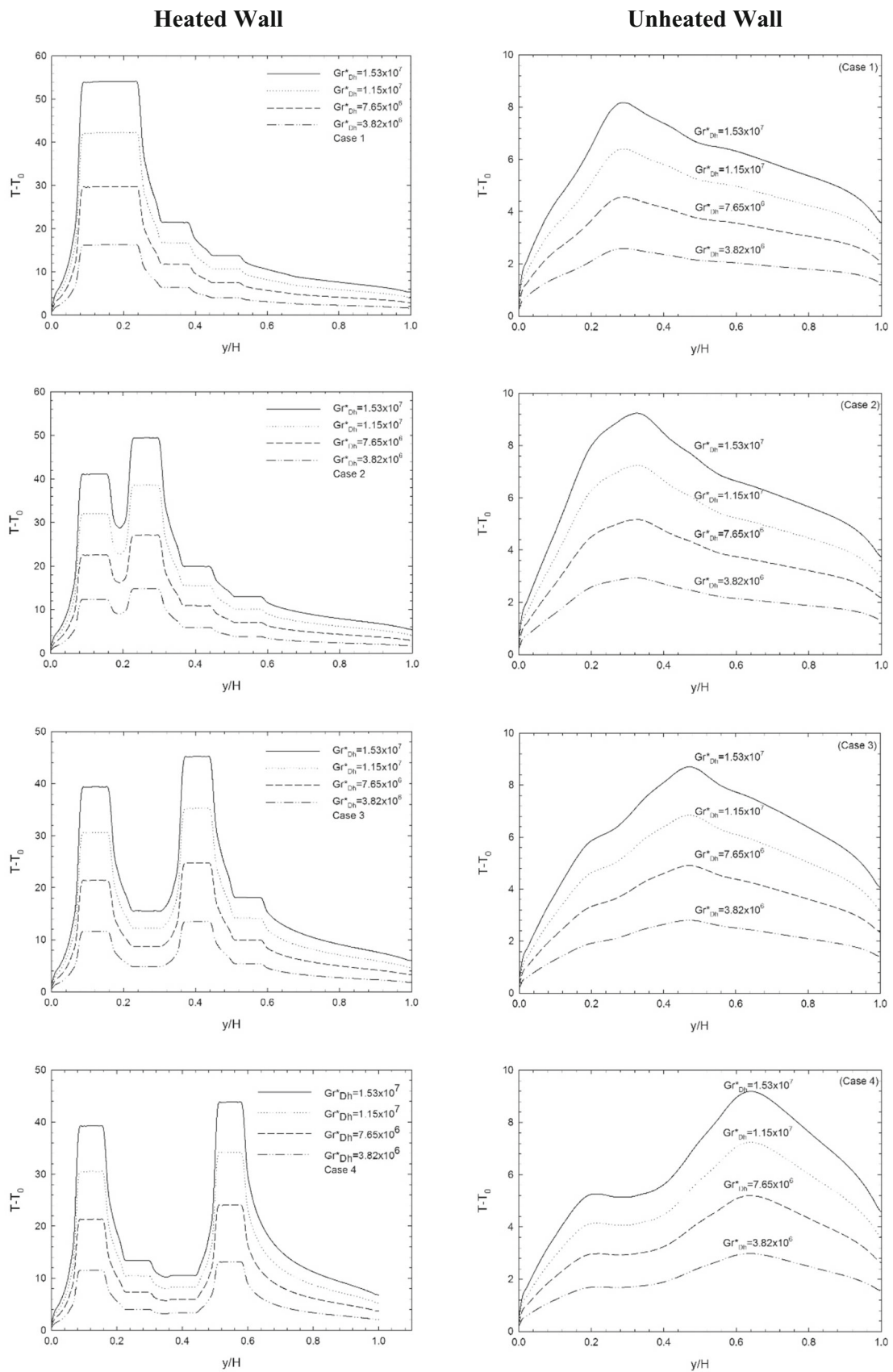
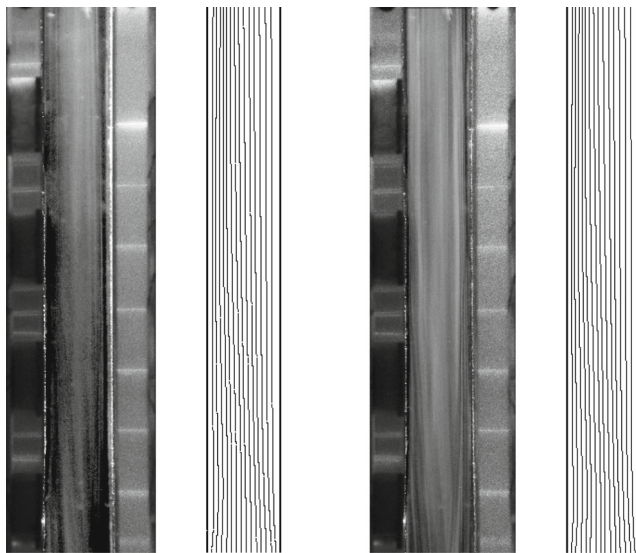


Fig. 7 Heated and unheated wall temperatures versus Gr_{Dh}^* for different cases



$$Gr_{Dh}^* = 9.56 \times 10^6$$

$$Gr_{Dh}^* = 1.53 \times 10^7$$

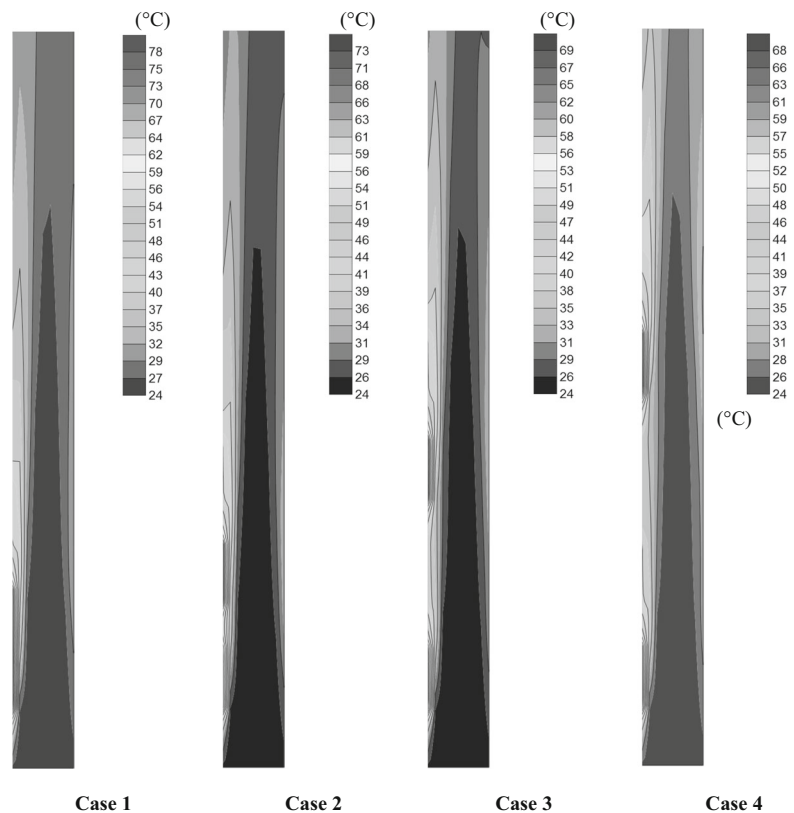
Fig. 8 Flow pattern at the inlet section for Case 2

where g is the gravitational acceleration, β is the thermal diffusivity, k is the thermal conductivity, ν is the kinematic viscosity of the fluid, q^* is the volumetric heat generation and t_h is the thickness of the heaters.

The hydraulic diameter of the channel is defined as:

$$D_h = \frac{4WD}{2(W + D)} \tag{2}$$

Fig. 9 Temperature contours at $Gr_{Dh}^* = 1.53 \times 10^7$



From the energy balance on the copper surfaces:

$$q_{conv} = q_{tot} - q_{cond} - q_{rad} \tag{3}$$

Here, q_{tot} is the total heat input, q_{cond} is the conduction heat loss and q_{rad} is the radiation heat loss from the copper surfaces.

The heat transfer coefficient on the heater surface is:

$$h = \frac{q_{conv}}{(T_s - T_0)} \tag{4}$$

where T_s and T_0 denote the surface temperature of the heater and ambient temperature of the air.

The local and average Nusselt numbers on the copper surfaces are calculated by following equations, respectively:

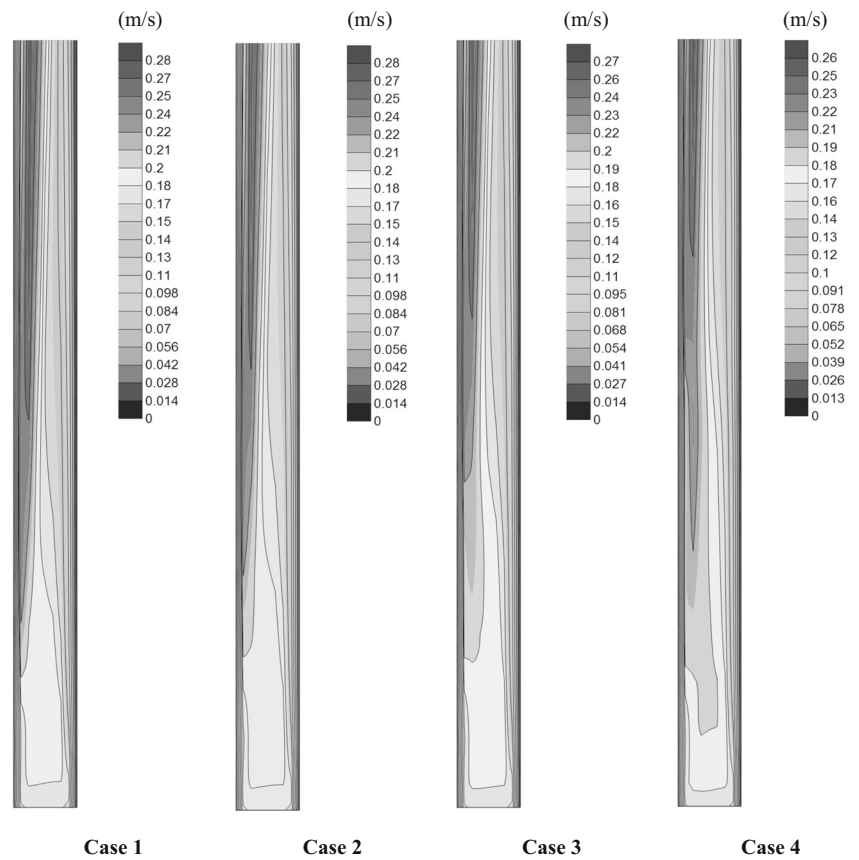
$$Nu = \frac{hD_h}{k_f} \tag{5}$$

$$Nu_{ave} = \frac{\bar{h}D_h}{k_f} \tag{6}$$

The Nusselt number ratio which gives the effectiveness of the heaters according to the 1st case is:

$$Nu_{eff} = \frac{Nu_{ave}}{Nu_{ave,case1}} \tag{7}$$

Fig. 10 Contours of the vertical velocity component at $Gr_{Dh}^* = 1.53 \times 10^7$



Pressure inlet and pressure outlet boundary conditions are used at the inlet and exit of the channel. Inlet and outlet pressures of the fluid are equal to the hydrodynamic pressure of the stagnant ambient air. No-slip boundary condition is used at the channel walls.

At the channel inlet:

$$p = p_0, T = T_0 \tag{8}$$

At the channel outlet:

$$p = p_0, \frac{\partial T}{\partial y} = 0 \tag{9}$$

Coupled boundary condition is used at all of the wall-to-fluid and wall-to-wall interfaces inside the channel where temperature and heat flux must be continuous, which is treated as:

$$-k_s \frac{\partial T}{\partial x} = -k_f \frac{\partial T}{\partial x} + q_{rad,net} \tag{10}$$

$$-k_{s1} \frac{\partial T}{\partial x} = -k_{s2} \frac{\partial T}{\partial x} \tag{11}$$

where s and f denote solid and fluid, respectively, and 1 and 2 represents different solid bodies. $q_{rad,net}$ denotes the net radiative heat flux from the boundary, and it is the difference of the outgoing and incoming radiation heat fluxes.

Convection flux boundary condition with the heat transfer coefficient of $h = 5 \text{ W/m}^2$ is implemented at the outer surfaces of the channel walls and insulation material.

For radiation calculations, external black body temperature is set to the reference temperature T_0 at the inlet-outlet boundaries, and internal emissivity value of these boundaries is 1. The emissivity value ϵ of the black channel surface and polished copper surfaces are 0.9 and 0.05, respectively.

Numerical computations are performed via ANSYS Fluent software based on the control volume method. Pressure based-segregated solver is used for incompressible flow. In this method, governing equations are solved sequentially. SIMPLE algorithm is used for the pressure-velocity coupling. Momentum and energy equations are discretized by a second order upwind scheme and pressure interpolation is provided by PRESTO scheme which is recommended for natural convection flows. The under relaxation factors for pressure, density, body forces, and momentum and energy equations are taken as 0.3, 1, 1, 0.7 and 1, respectively. In the numerical computations, the thermophysical properties of air are assumed to be constant and the ambient temperature at 24°C is taken as reference. Radiation heat exchange between the surfaces is taken into account by

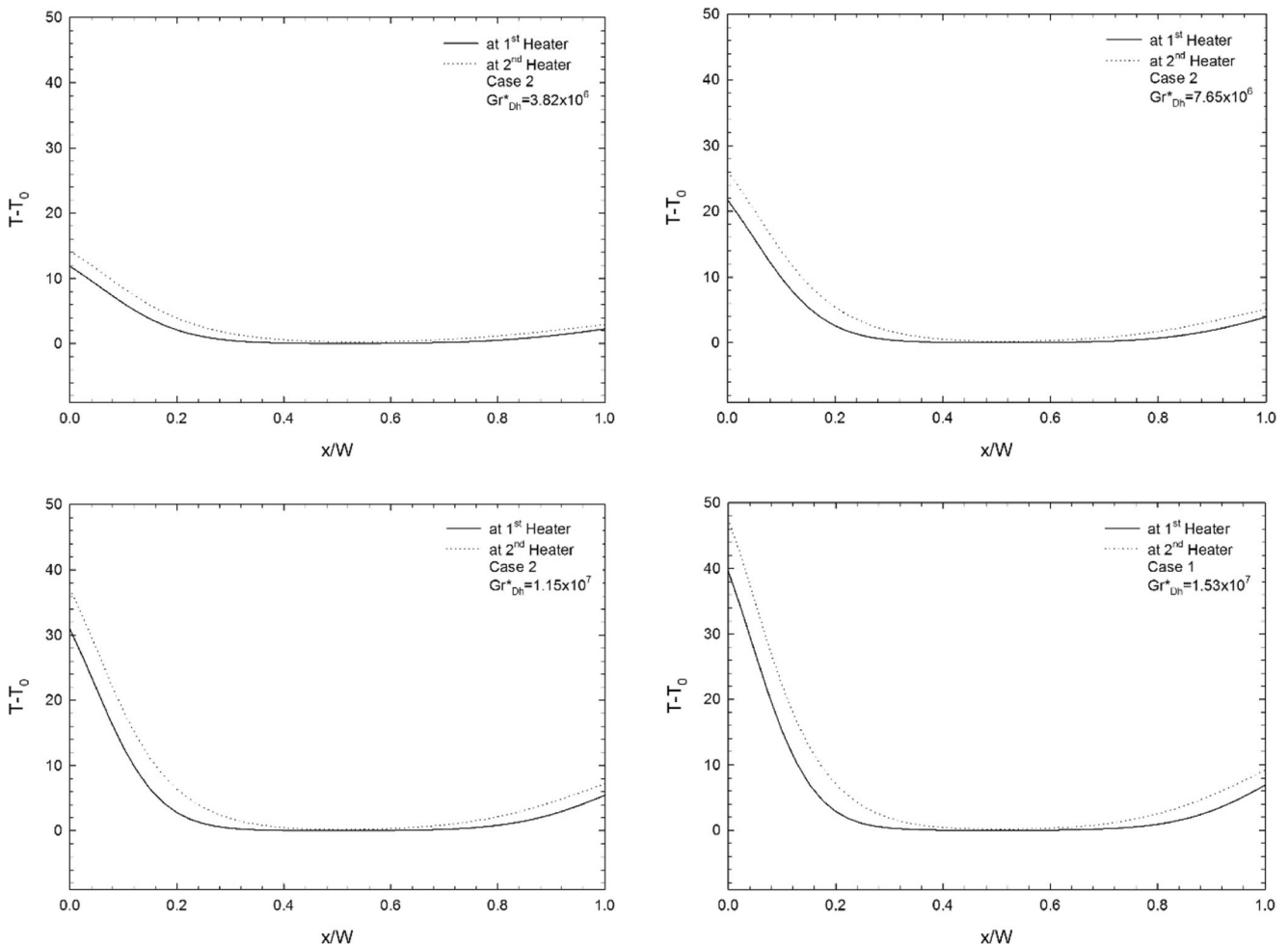


Fig. 11 Variation of the temperature in the horizontal direction at the trailing edges of the heaters at various values of Gr_{Dh}^* (Case 2)

surface to surface radiation method (S2S) which assumes the surfaces gray and diffuse. View factors are calculated by the program using a face to face basis and ray tracing method. More information about the numerical model can be found in Ref. [35, 37]. The convergence criterion is set to 10^{-5} for the continuity, momentum, energy and S2S model eqs.

A non-uniform grid structure is employed in the solution domain. In order to encounter higher gradients within the boundary layers accurately, finer grid is adopted in the flow field, interior of the heaters and channel walls. The grid is denser in the x -direction while coarse grid covers the y and z -directions. Grid size is successively refined until two successive grid size present negligible differences in the corresponding output parameters. Four different grid structures consisting of $20 \times 300 \times 30$, $40 \times 300 \times 30$, $60 \times 300 \times 30$ and $80 \times 300 \times 30$ cells in the flow field are comparatively tested, which correspond to the following cell numbers: 1,265,616, 1,736,856, 2,235,024 and 2,706,264. Tests showed that grid size of $40 \times 300 \times 30$ is adequate for

grid-independent solutions. The grid structure is shown in Fig. 4.

Grid independent numerical results were compared against the experimental results on the heated and unheated walls for the Case 2 defined below. Temperature values on the heated sidewall are represented as the temperature difference between the temperatures of measurement points and reference ambient temperature (T_0). It is clearly seen from Fig. 5 that numerical results agree fairly well with our experimental measurements, and maximum difference between numerical results and experimental measurements is about 3.1%.

4 Results and discussion

An experimental and numerical study of natural convection heat transfer in a discretely heated vertical channel is performed. Four different cases are tested (see Fig. 6). Two heaters are combined at the entrance of the channel, and they behave like a single heater (Case 1). Two discrete heaters are placed discretely with the distance of

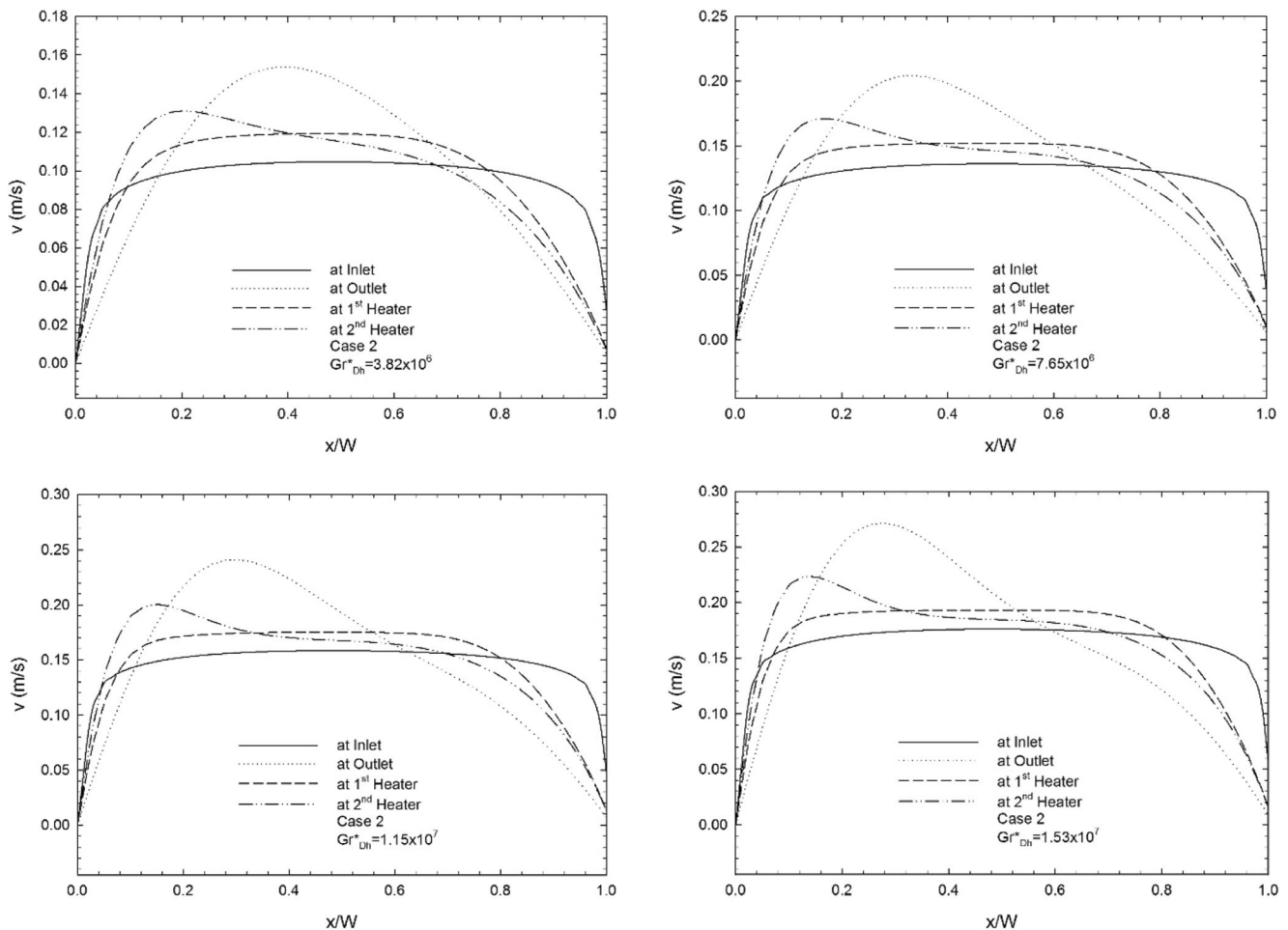


Fig. 12 Variation of the vertical velocity component in the horizontal direction at different locations at various values Gr_{Dh}^* (Case 2)

19.05 mm (Case 2), 63.50 mm (Case 3) and 107.95 mm (Case 4). The experimental study covers four different values of the modified Grashof number ($Gr_{Dh}^* = 9.56 \times 10^6, 1.15 \times 10^7, 1.34 \times 10^7, 1.53 \times 10^7$) while the numerical ones are in the range of 9.6×10^5 and 1.53×10^7 .

Figure 7 illustrates temperature variations at the heated and unheated walls for different values of Gr_{Dh}^* . The copper surfaces are heated at the back with flexible heaters in the experimental study, which is simulated with volumetric heat generation in the numerical part. Gr_{Dh}^* is also a function of volumetric heat generation. Hence, surface temperatures of the heaters and unheated parts of the channel wall increase with Gr_{Dh}^* , as expected. It is seen from the figure, surface temperature rises sharply from the entrance of the channel, and temperature of the heater remains uniform due to the high conductivity of the copper plate. Surface temperatures are higher due to the heat generation on the heater surface, and they decrease towards the channel exit. Air entering the channel at ambient temperature (24°C) is heated by contacting the heater

surfaces and moves upward under the influence of buoyancy force. The second heater has a higher temperature since cooling air temperature increases when fluid moves upward. As it is clearly seen, the clearance between the heaters has a significant influence on the surface temperatures and heat transfer.

Radiation heat exchange has a remarkable effect on natural convection, and it aids the buoyancy induced flow. The unheated opposing wall temperature varies depending on the temperatures of the heaters. This becomes obvious especially at higher values of Gr_{Dh}^* . Surface temperature increase with Gr_{Dh}^* , taking the highest value at the opposite of the second heater. The highest temperature on the unheated wall shifts towards the channel exit with an increase in the clearance between the heaters.

As an example, the streamline patterns obtained experimentally and numerically at the center ($D = 76.2$ mm) of the channel depth for $Gr_{Dh}^* = 9.56 \times 10^6$ and $Gr_{Dh}^* = 1.53 \times 10^7$ are shown in Fig. 8, for Case 2. Depending on the increase in fluid temperature, buoyancy effects become significant, and air ascends along the channel. The

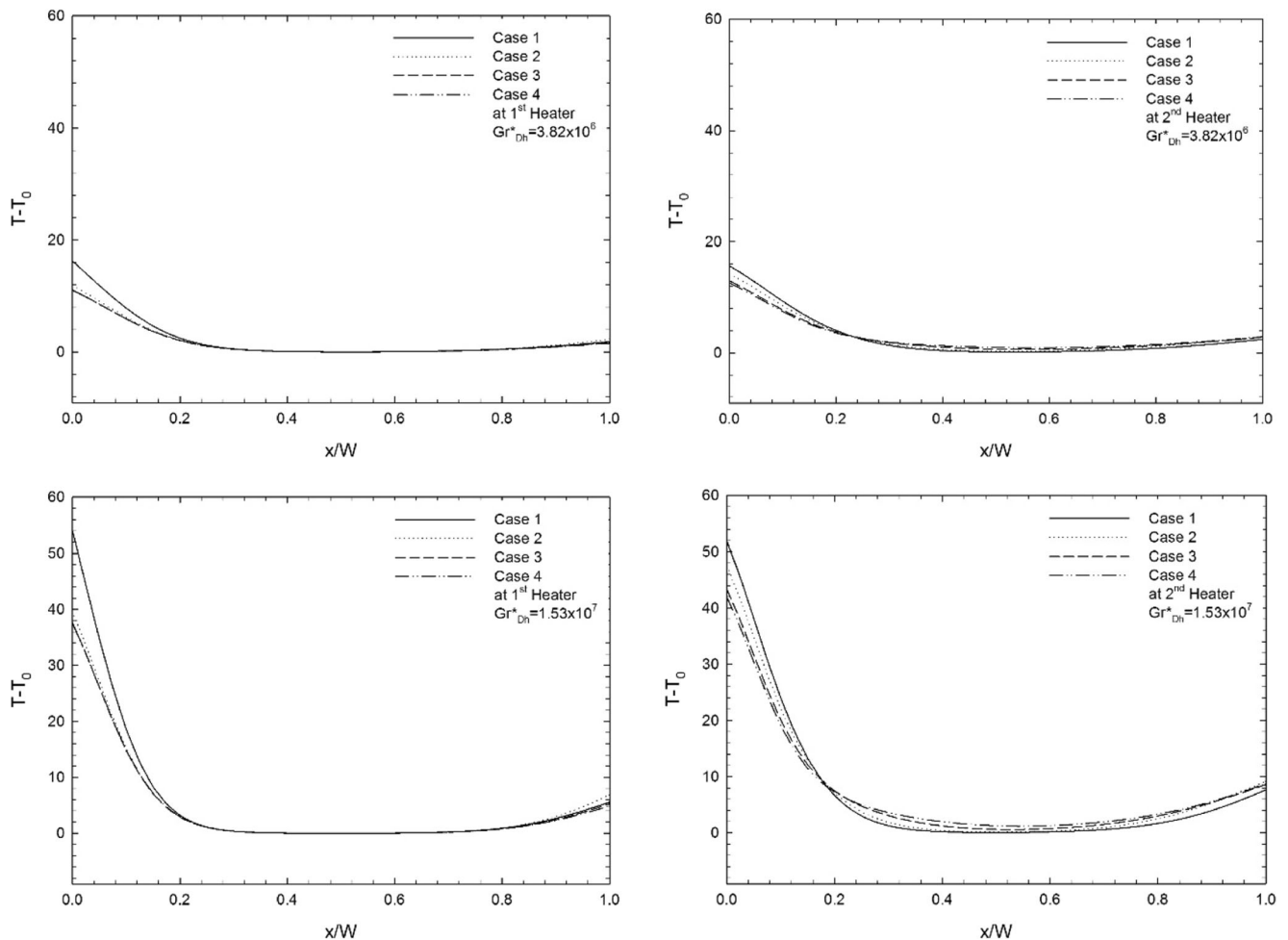


Fig. 13 Variation of the temperature in the horizontal direction at the trailing edges of the heaters at various values of Gr_{Dh}^*

surface temperature of the unheated wall increases due to radiation heat transfer between channel walls, and this causes streamlines to be parallel to the surfaces. Previously, we investigated the effects of surface radiation by setting the surface emissivities to zero [29]. Flow reversal was obtained near the unheated wall when the surface radiation was not taken into account. Similar observations were made by others [8, 19], too.

For $Gr_{Dh}^* = 1.53 \times 10^7$ isotherms are shown in Fig. 9. It is seen that the isotherms become denser in the vicinity of the heaters. Thermal boundary layer is thinner at the entrance region and gradually increases along the channel. Therefore, convective heat transfer rate from the first heater to the air is higher than the second heater. With an increase in the heater clearance, air cools down before contacting the second heater. Thus, convective heat transfer increases, and maximum temperature value in the flow domain decreases by 10°C . In addition, temperature of the unheated wall increases due to the radiation heat exchange.

Figure 10 illustrates the vertical velocity contours for $Gr_{Dh}^* = 1.53 \times 10^7$. When air contacts with the heater, it

accelerates as a result of buoyancy forces. Velocity of the air near the heaters increases with the buoyancy forces, which results in an asymmetric velocity distribution in the channel. Vertical velocity component takes the highest value just above the second heater. This point moves upward and the maximum velocity decreases with increasing distance between the heaters. Additionally, as it can be seen from the streamlines, no reverse flow is observed in the channel.

Temperature variation in the horizontal direction at the trailing edges of the heaters is shown in Fig. 11 for Case 2. Although the temperature is almost equal to the inlet temperature at large part of the channel, higher temperatures are observed in the vicinity of the heaters. Heat transfer from the first heater is higher than the second heater, which can be discernable from the boundary layer structure. The thermal boundary layer is thinner at the trailing edge of the first heater, and this situation becomes more evident as Gr_{Dh}^* increases. As a result of the radiation heat exchange between the surfaces, temperature of the right surface increases, and the temperature of the air

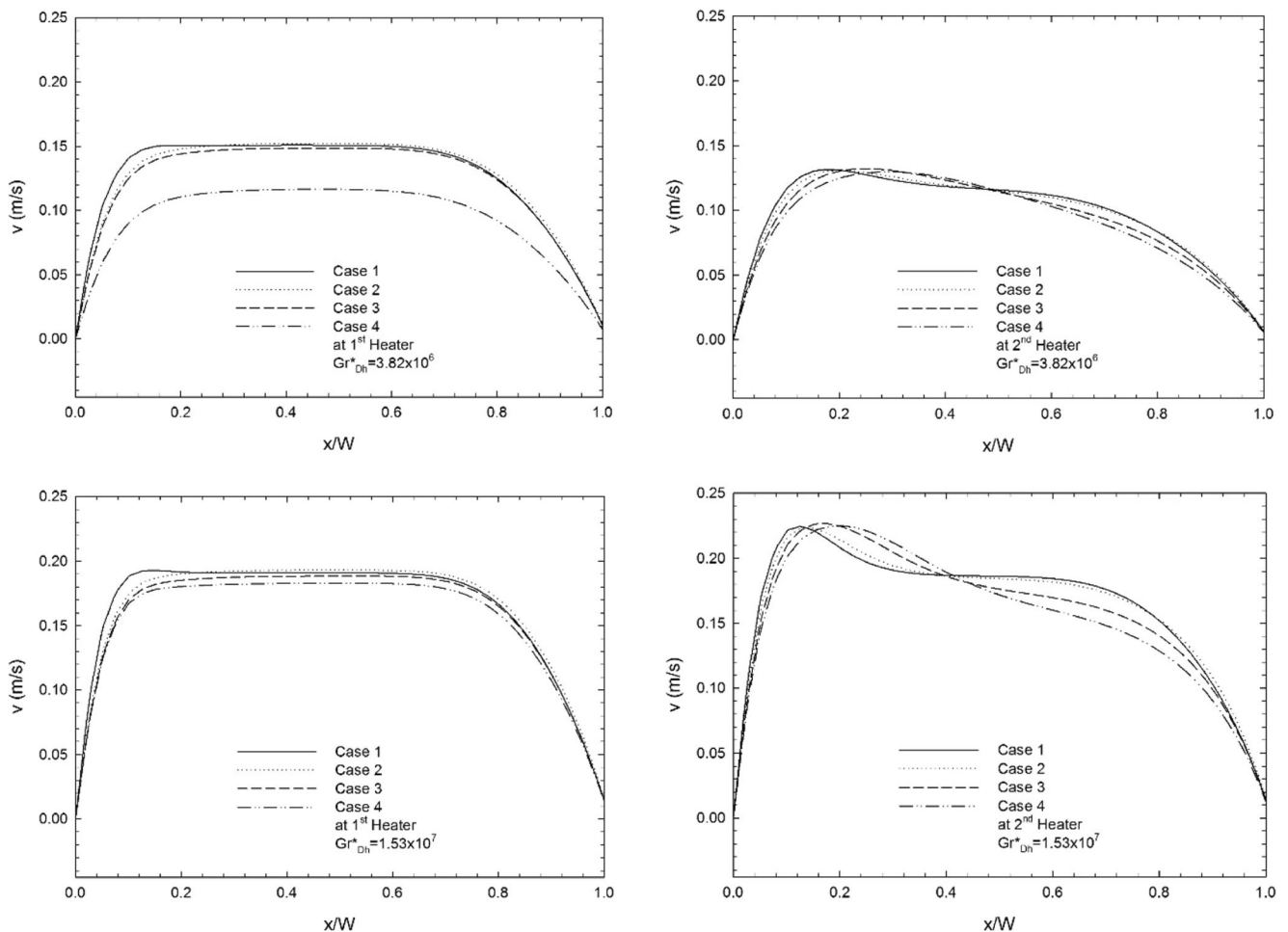


Fig. 14 Variation of the vertical velocity component in the horizontal direction at the trailing edges of the heaters at various values of Gr_{Dh}^*

near the surface also increases, especially for higher values of Gr_{Dh}^* .

Effect of Gr_{Dh}^* on vertical velocity distribution at different stations is illustrated in Fig. 12 for Case 2. Due to enhanced buoyancy effects as a result of the temperature rise, air ascends along the channel, and velocity values become higher near the heated wall. An asymmetric velocity distribution is observed with an increase in Gr_{Dh}^* . This situation is especially noticeable at the trailing edge of the second heater where the air temperature is high.

Temperature and velocity variations in the horizontal directions at the trailing edge of the heaters are shown in Figs. 13 and 14. As it is seen from the figure, temperature distributions are almost uniform especially for low values of Gr_{Dh}^* at the trailing edge of the first heater. When the trailing edge of the second heater is examined, it is seen that the clearance between the heaters is an important parameter influencing air flow and heat transfer. This becomes more apparent as Gr_{Dh}^* increases. In all the cases examined, velocity profile is

almost symmetrical, and velocity values are low at the first heater zone. In the second heater zone, together with the temperature rise, the effect of the buoyancy forces becomes important, the symmetry breaks down and boundary layer formation is seen more clearly (see Fig. 14).

Figure 15 shows the variation of the local Nusselt number Nu along the heater surfaces for various values of Gr_{Dh}^* . Nu takes its maximum value at the leading edge of the heaters, and it then decreases along the heater surface taking its minimum value at the trailing edge of the heater. This trend becomes more apparent with an increase in Gr_{Dh}^* . For Case 1, Nu is maximum at the leading edge compared to the other cases but its value is lower at the trailing edge. This is due to the overheating of the heaters since there is no clearance between the heaters. As the clearance between the heaters increases, convective heat transfer from the second heater increases.

Figure 16 illustrates the hot spot temperature variation with Gr_{Dh}^* . The maximum temperature reached is

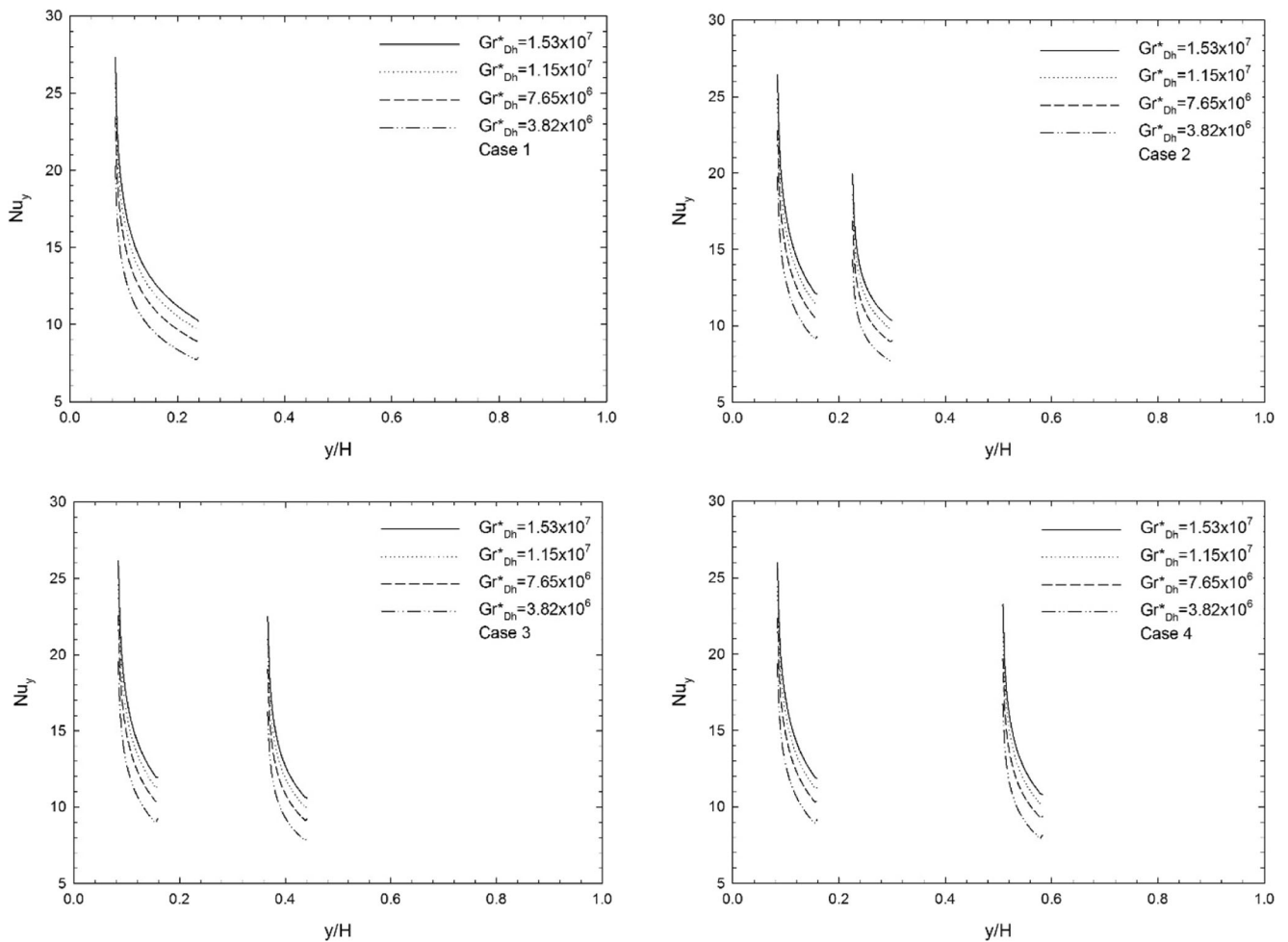


Fig. 15 The variation of the local Nusselt number Nu with Gr_{Dh}^*

called as hot spot temperature [31]. The hot spot temperature is observed to depend on the heater clearance and Gr_{Dh}^* . In order to investigate the effect of heater clearance on convective heat transfer from the heaters,

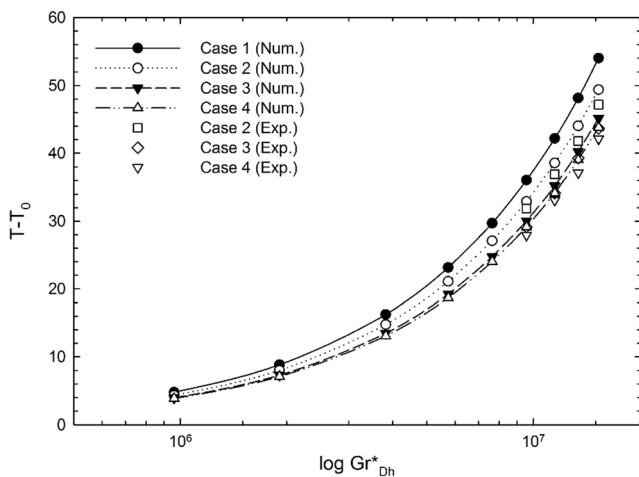
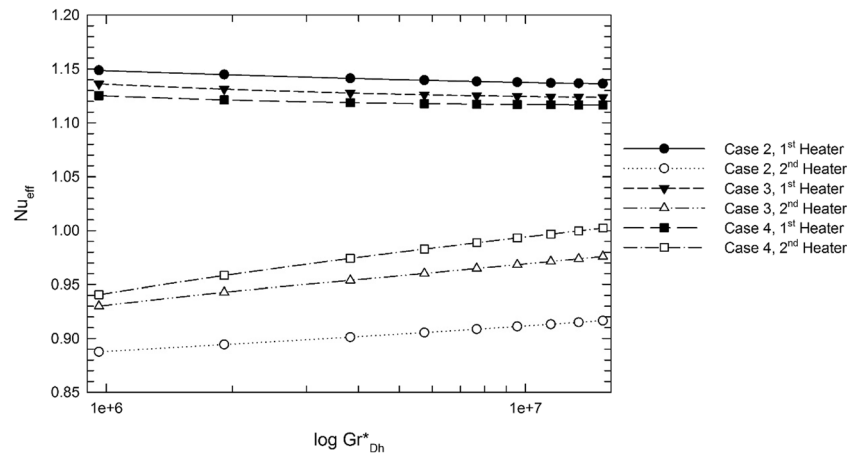


Fig. 16 The variation of the hot spot temperature with Gr_{Dh}^*

the total heater length is kept constant. It is seen from the figure that hot spot temperatures are close to each other for lower values of Gr_{Dh}^* , and there is no significant difference in temperature values, which is an indication of uniform cooling. The effect of the heater clearance becomes more apparent with an increase in Gr_{Dh}^* . For all the values of Gr_{Dh}^* , hot spot temperature takes its highest value for Case 1 while the lowest value is obtained for Case 4. For a fixed heater length, increasing the heater clearance enhances heat transfer from the heaters.

The variation of the effective Nusselt number Nu_{eff} with Gr_{Dh}^* is shown in Fig. 17. The effective Nusselt number is defined as the ratio of the average Nusselt numbers calculated on heater surfaces in any case to that in the Case 1. This ratio indicates how effective the heaters are when compared with the first case. It is seen that Nu_{eff} decreases with an increase in Gr_{Dh}^* for the first heater. Surface temperatures are higher for Case 1, especially for higher values of Gr_{Dh}^* . When the second heaters are considered, heat transfer increases with the

Fig. 17 The variation of the effective Nusselt number Nu_{eff} with Gr_{Dh}^*



clearance and Gr_{Dh}^* . When Figs. 15 and 16 are examined together, it is clear that convective heat transfer increases with the distance between the heaters, which results in more efficient cooling.

The results show that an increase in the modified Grashof number or in the clearance between the heaters increases the average Nusselt number. As a result of the numerical calculations, a correlation equation was developed to predict the variation of the average Nusselt number with the modified Grashof number and the dimensionless clearance between the heaters as follows:

$$Nu_{ave,1} = 0.4867(Gr_{Dh}^*)^{0.2082}(s/L_{tot})^{-0.0105} \quad (12)$$

$$Nu_{ave,2} = 0.3312(Gr_{Dh}^*)^{0.2286}(s/L_{tot})^{0.0484} \quad (13)$$

The maximum and minimum errors between computed and correlated values by Eqs. 12 and 13 are 1.46 and 0.021%, respectively.

5 Conclusions

Some of the important findings obtained in the study can be summarized as follows:

- Surface temperatures of the heated walls increase from the entrance and decrease towards the exit in all the cases examined. They are also shown to be affected from the surface radiation.
- Surface radiation significantly affect flow and heat transfer by aiding the buoyancy forces.
- It is disclosed that increasing the clearance between the heat sources enhances convective heat transfer from the second heater. It is also shown to decrease the hot spot

temperature. This situation becomes more pronounced with an increase in the modified Grashof number.

Acknowledgements This study is supported by The Scientific and Technological Research Council of Turkey (TUBITAK) with project number of 114 M589.

Compliance with ethical standards

Conflict of interest statement On behalf of all authors, Prof. Orhan Aydin, the corresponding author of this article states that there is no conflict of interest.

References

1. Yan W, Lin T (1987) Natural convection heat transfer in vertical open channel flows with discrete heating. *Int Commun Heat Mass Transfer* 14:187–200. [https://doi.org/10.1016/s0735-1933\(87\)81009-6](https://doi.org/10.1016/s0735-1933(87)81009-6)
2. McEntire A, Webb B (1990) Local forced convective heat transfer from protruding and flush-mounted two-dimensional discrete heat sources. *Int J Heat Mass Transf* 33:1521–1533. [https://doi.org/10.1016/0017-9310\(90\)90048-y](https://doi.org/10.1016/0017-9310(90)90048-y)
3. Chadwick M, Webb B, Heaton H (1991) Natural convection from discrete heat sources in a vertically vented rectangular enclosure. *Exp Heat Transfer* 4:199–216. <https://doi.org/10.1080/08916159108946414>
4. Elpidorou D, Prasad V, Modi V (1991) Convection in a vertical channel with a finite wall heat source. *Int J Heat Mass Transf* 34:573–578. [https://doi.org/10.1016/0017-9310\(91\)90274-i](https://doi.org/10.1016/0017-9310(91)90274-i)
5. Choi C, Ortega A (1993) Mixed convection in an inclined channel with a discrete heat source. *Int J Heat Mass Transf* 36:3119–3134. [https://doi.org/10.1016/0017-9310\(93\)90040-d](https://doi.org/10.1016/0017-9310(93)90040-d)
6. Yucel C, Hasnaoui M, Robillard L, Bilgen E (1993) Mixed convection heat transfer in open ended inclined channels with discrete isothermal heating. *Numer Heat Transfer, Part A* 24:109–126. <https://doi.org/10.1080/10407789308902605>
7. Mishra D, Muralidhar K, Ghoshdastidar P (1995) Computation of flow and heat transfer around a vertical discrete protruding heater using an operator-splitting algorithm. *Numer Heat Transfer, Part A* 28:103–119. <https://doi.org/10.1080/10407789508913735>

8. Turkoglu H, Yucel N (1995) Mixed convection in vertical channels with a discrete heat source. *Heat Mass Transf* 30:159–166. <https://doi.org/10.1007/bf01476525>
9. Fujii M, Gima S, Tomimura T, Zhang X (1996) Natural convection to air from an array of vertical parallel plates with discrete and protruding heat sources. *Int J Heat Fluid Flow* 17:483–490. [https://doi.org/10.1016/0142-727x\(96\)00051-3](https://doi.org/10.1016/0142-727x(96)00051-3)
10. Du S, Bilgen E, Vasseur P (1998) Mixed convection heat transfer in open ended channels with protruding heaters. *Heat Mass Transf* 34:263–270. <https://doi.org/10.1007/s002310050258>
11. Xu G, Tou K, Tso C (1998) Numerical modelling of turbulent heat transfer from discrete heat sources in a liquid-cooled channel. *Int J Heat Mass Transf* 41:1157–1166. [https://doi.org/10.1016/s0017-9310\(97\)00257-3](https://doi.org/10.1016/s0017-9310(97)00257-3)
12. Tsay Y (1999) Transient conjugated mixed-convective heat transfer in a vertical plate channel with one wall heated discretely. *Heat Mass Transf* 35:391–400. <https://doi.org/10.1007/s002310050341>
13. Bessaih R, Kadja M (2000) Turbulent natural convection cooling of electronic components mounted on a vertical channel. *Appl Therm Eng* 20:141–154. [https://doi.org/10.1016/s1359-4311\(99\)00010-1](https://doi.org/10.1016/s1359-4311(99)00010-1)
14. Rao C, Balaji C, Venkateshan S (2001) Conjugate mixed convection with surface radiation from a vertical plate with a discrete heat source. *ASME J Heat Transfer* 123:698. <https://doi.org/10.1115/1.1373654>
15. Gururaja Rao C, Balaji C, Venkateshan S (2002) Effect of surface radiation on conjugate mixed convection in a vertical channel with a discrete heat source in each wall. *Int J Heat Mass Transf* 45:3331–3347. [https://doi.org/10.1016/s0017-9310\(02\)00061-3](https://doi.org/10.1016/s0017-9310(02)00061-3)
16. Rao C (2004) Buoyancy-aided mixed convection with conduction and surface radiation from a vertical electronic board with a traversable discrete heat source. *Numer Heat Transfer, Part A* 45:935–956. <https://doi.org/10.1080/10407780490439202>
17. Manca O, Nardini S, Naso V (2002) Effect on natural convection of the distance between an inclined discretely heated plate and a parallel shroud below. *ASME J Heat Transfer* 124:441. <https://doi.org/10.1115/1.1470488>
18. Mathews R, Balaji C, Sundararajan T (2007) Computation of conjugate heat transfer in the turbulent mixed convection regime in a vertical channel with multiple heat sources. *Heat Mass Transf* 43:1063–1074. <https://doi.org/10.1007/s00231-006-0192-9>
19. Desrayaud G, Fichera A, Lauriat G (2007) Natural convection air-cooling of a substrate-mounted protruding heat source in a stack of parallel boards. *Int J Heat Fluid Flow* 28:469–482. <https://doi.org/10.1016/j.ijheatfluidflow.2006.07.003>
20. Rao G, Narasimham G (2007) Laminar conjugate mixed convection in a vertical channel with heat generating components. *Int J Heat Mass Transf* 50:3561–3574. <https://doi.org/10.1016/j.ijheatmasstransfer.2006.12.030>
21. Sawant S, Gururaja Rao C (2008) Conjugate mixed convection with surface radiation from a vertical electronic board with multiple discrete heat sources. *Heat Mass Transf* 44:1485–1495. <https://doi.org/10.1007/s00231-008-0395-3>
22. Guimaraes P, Menon G (2008) Combined free and forced convection in an inclined channel with discrete heat sources. *Int Comm Heat Mass Transfer* 35:1267–1274. <https://doi.org/10.1016/j.ijheatmasstransfer.2008.08.006>
23. Boutina L, Bessaih R (2011) Numerical simulation of mixed convection air-cooling of electronic components mounted in an inclined channel. *Appl Therm Eng* 31:2052–2062. <https://doi.org/10.1016/j.applthermaleng.2011.03.021>
24. Laouche N, Korichi A, Popa C, Polidori G (2016) Laminar aiding and opposing mixed convection in a vertical channel with an asymmetric discrete heating at one wall. *Therm Sci* 149–149. <https://doi.org/10.2298/tsci1601051491>
25. Premachandran B, Balaji C (2011) Conjugate mixed convection with surface radiation from a vertical channel with protruding heat sources. *Numer Heat Transfer, Part A* 60:171–196. <https://doi.org/10.1080/10407782.2011.588577>
26. Kumar Ganesh G, Gururaja Rao C (2011) Parametric studies and correlations for combined conduction-mixed convection-radiation from a non-identically and discretely heated vertical plate. *Heat Mass Transf* 48:505–517. <https://doi.org/10.1007/s00231-011-0899-0>
27. Gavara M (2012) Natural convection in a vertical channel with arrays of flush-mounted heaters on opposite conductive walls. *Numer Heat Transfer, Part A* 62:111–135
28. Londhe S, Gururaja Rao C (2014) Interaction of surface radiation with conjugate mixed convection from a vertical channel with multiple discrete heat sources. *Heat Mass Transf* 50:1275–1290. <https://doi.org/10.1007/s00231-014-1333-1>
29. Sarper B, Saglam M, Aydin O, Avci M (2017) Natural convection heat transfer from discretely heated vertical channel: effect of the surface radiation. *Proceedings of the 2nd World Congress on Momentum, Heat and Mass Transfer (MHMT'17)*. [10.11159/enfht17.106](https://doi.org/10.11159/enfht17.106)
30. Chen S, Liu Y, Chan S, Leung C, Chan T (2001) Experimental study of optimum spacing problem in the cooling of simulated electronic package. *Heat Mass Transf* 37:251–257. <https://doi.org/10.1007/s002310000168>
31. da Silva A, Lorente S, Bejan A (2004) Optimal distribution of discrete heat sources on a wall with natural convection. *Int J Heat Mass Transf* 47:203–214. <https://doi.org/10.1016/j.ijheatmasstransfer.2003.07.007>
32. da Silva A, Lorenzini G, Bejan A (2005) Distribution of heat sources in vertical open channels with natural convection. *Int J Heat Mass Transf* 48:1462–1469. <https://doi.org/10.1016/j.ijheatmasstransfer.2004.10.019>
33. Holman JP (2010) *Heat transfer*, 10th edn. The McGraw-Hill Companies, Inc, New York
34. Holman JP (2012) *Experimental methods for engineers*, 8th edn. The McGraw-Hill Companies, Inc, New York
35. ANSYS Fluent (2013) Release 15.0, Theory Guide. ANSYS Inc, Pittsburgh
36. Oosthuizen PH, Naylor D (1999) *An introduction to convective heat transfer analysis*. The McGraw-Hill Companies, Inc, New York
37. Siegel R, Howell J (2002) *Thermal radiation heat transfer*, 4th edn. Taylor & Francis, New York